A Journal of the Gesellschaft Deutscher Chemiker

Angewandte International Edition GDCh Chemie

www.angewandte.org

Accepted Article

Title: Paired electrocatalytic oxygenation and hydrogenation of organic substrates using water as oxygen and hydrogen source

Authors: Licheng Sun, Peili Zhang, Xia Sheng, Xiaoyu Chen, Zhiyong Fang, Jian Jiang, Mei Wang, Fusheng Li, Lizhou Fan, Yansong Ren, Biaobiao Zhang, Brian Timmer, and Marten Ahlquist

To be cited as: *Angew. Chem. Int. Ed.* 10.1002/anie.201903936
Angew. Chem. 10.1002/ange.201903936

Link to VoR: http://dx.doi.org/10.1002/anie.201903936
http://dx.doi.org/10.1002/ange.201903936

WILEY-VCH

10.1002/anie.201903936

WILEY-VCH

COMMUNICATION

Paired electrocatalytic oxygenation and hydrogenation of organic substrates using water as oxygen and hydrogen source

Peili Zhang,[a,b] Xia Sheng,[a] Xiaoyu Chen,[c] Zhiyong Fang,[b] Jian Jiang,[b] Mei Wang,[b] Fusheng Li,[b] Lizhou Fan,[a] Yansong Ren,[a] Biaobiao Zhang,[a] Brian J.J. Timmer,[a] Mårten S.G.Ahlquist,[c] Licheng Sun*[a,b]

Abstract: The use of water as an oxygen and hydrogen source for the paired oxygenation and hydrogenation of organic substrates to produce valuable chemicals is of utmost importance as a means of establishing green chemical syntheses. Inspired by the active Ni^{3+} intermediates involved in electrocatalytic water oxidation by Ni-based materials, we prepared NiB_x as a catalyst and used water as the oxygen source for the oxygenations of various organics. NiB_x was further employed as both an anode and cathode in a paired electrosynthesis cell for the respective oxygenation and hydrogenation of organic compounds, with water as both the oxygen and hydrogen source. Conversions efficiencies and selectivities of ≥99% were achieved during the oxygenation of 5-hydroxymethylfurfural to 2,5-furandicarboxylic acid and the simultaneous hydrogenation of *p*-nitrophenol to *p*-aminophenol. This paired electrosynthesis cell has also been coupled to a solar cell as a stand-alone reactor in response to sunlight.

Water is an abundant resource on earth and is widely used as either an oxygen or hydrogen source during naturally occurring biosynthetic oxygenation and hydrogenation reactions.[1,2] Inspired by natural systems, we consider water to represent an ideal source of oxygen and hydrogen instead of high-cost H_2 or chemical oxidants/reductants for catalytic oxygenation and hydrogenation in green chemical processes.

During the last decade, electrocatalytic oxygenation of organic compounds to value-added products with water as oxygen source has started to attract increased attention. Several interesting electrocatalytic systems have been reported with improving performance. Ni_2P,[3a] Co-P, [3b] Ni_3S_2, [3c] Ni_xB, [3d] NiFe LDH, [3e] noble metals (Au and Pd) and their alloys[3f] are used as efficient electrocatalysts for the oxidation of furanics and other biomass-derived platform chemicals. Recently, Schuhmann group provided new insight into the oxidation pathway of 5-hydroxymethylfurfural (HMF) through *operando* electrochemistry coupled attenuated total reflection infrared spectroscopy with Ni_xB as the catalyst.[3d] To date, the majority of literature reports have focused on conversions efficiencies and selectivities, while the water active process, the catalytic active sits and the oxygen atom transfer mechanism are ambiguity. [3]

In electrocatalytic oxygenation reactions, protons are generated as a by-product.[4] Recently, these reactions have been paired with electrocatalytic hydrogen evolution reaction (HER) to increase the energy conversion efficiency.[3] However, compared with HER, the organic oxygenation reactions are kinetically sluggish, especially in the late stages of the reaction, owing to the decrease in reactant concentrations. Thus, both catalytic efficiency and electron economy could be improved by pairing organic oxygenation with a rate-matched organic hydrogenation to create sustainable chemical synthesis strategies.[4]

Herein, the electrocatalytic oxygen atom transfer mechanism was investigated in 1 M KOH with NiB_x (x = 0.40 ± 0.05) as catalyst and the oxygenation of HMF to 2,5-furandicarboxylic acid (FDCA) as a model reaction. Experiment results indicated that the electrogenerated Ni^{3+} species are the active intermediates. Furthermore, paired electrolysis system was constructed by combining the electrocatalytic oxygenation of HMF to FDCA and the hydrogenation of *p*-nitrophenol (*p*-NP) to *p*-aminophenol (*p*-AP). Conversions efficiencies, selectivities and faradic efficiency as high as ≥99% were achieved on both sides with water as oxygen and hydrogen source. This paired electrolyser uses electricity to drive the organic oxygenation and hydrogenation reactions in aqueous solutions, without the need to handle hazardous gaseous hydrogen or oxygen or to incorporate external oxidants/ reductants.

The NiB_x working electrode (WE) was prepared by electroless plating for 2 hours with a nickel foam (NF) substrate at 90 °C in NaOH aqueous solutions (pH 13.5) containing $Ni(Cl)_2{\cdot}6H_2O$ (125 mM), ethanediamine (750 mM) and $NaBH_4$ (55 mM).[5] The Ni:B atomic ratio (1:0.40 ± 0.05) was verified by inductively coupled plasma optical emission spectroscopy and the NiB_x loading on the NF surface was 2.47 ± 0.10 mg cm^{-2}. Top-view scanning electron microscopy (SEM) images showed that NiB_x was uniformly deposited on the NF to provide a rough surface (**Figures 1a, 1b**). High-resolution transmission electron microscopy (TEM) images (**Figure 1c**) suggested that the surface particles were composed of amorphous nickel boride and nickel. X-ray photoelectron spectroscopy (XPS) analysis confirmed that Ni and B were the main components (**Figure S1**). The Ni $2p_{3/2}$ peak at 852.7 eV can be assigned to Ni^0, while the B 1s peak at 187.8 eV can be assigned to B^0, as expected for nickel borides.[6] The weak B 1s hump at 192.1 eV and the O 1s peak at 532.5 eV are due to small amounts of boron oxide (**Figures 1j-l**).[6b]

[a] Dr. P. Zhang, Dr. X. Sheng, L. Fan, Dr. Y. Ren, Dr. B. Zhang, Dr. B.J.J. Timmer, and Prof. L. Sun, Department of Chemistry, School of Engineering Sciences in Chemistry, Biotechnology and Health, KTH Royal Institute of Technology, 10044 Stockholm, Sweden E-mail: lichengs@kth.se

[b] Dr. P. Zhang, Z. Fang, J. Jiang, Prof. M. Wang, Dr. F. Li, and Prof. L. Sun, State Key Laboratory of Fine Chemicals, Institute of Artificial Photosynthesis, DUT-KTH Joint Education and Research Centre on Molecular Devices, Dalian University of Technology, 116024 Dalian, China

[c] X. Chen and Dr. M.S.G. Ahlquist, Department of Theoretical Chemistry & Biology, School of Engineering Sciences in Chemistry Biotechnology and Health, KTH Royal Institute of Technology, 10691 Stockholm, Sweden

Supporting information for this article is given via a link at the end of the document.

10.1002/anie.201903936

WILEY-VCH

COMMUNICATION

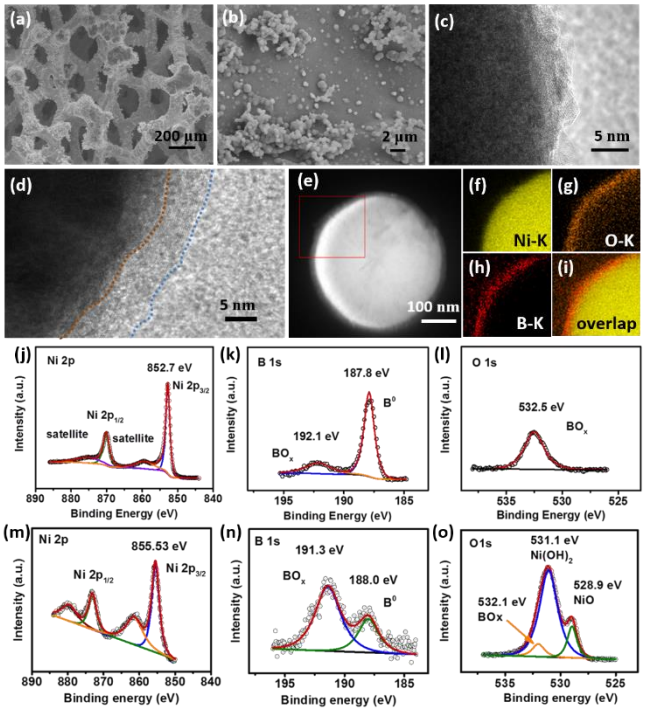

Figure 1. (a,b) SEM images and (c) TEM image of the as-prepared NiBx@NF; (d) TEM image and (e‑i) elemental mapping of NiB_x@NF after controlled potential electrolysis at 0.50 V vs. SHE; (j‑l) high-resolution (j) Ni 2p, (k) B 1s and (l) O 1s XPS spectra obtained from the as-prepared NiB_x@NF; (m‑o) high-resolution (m) Ni 2p, (n) B 1s and (o) O 1s XPS spectra obtained from the NiB_x@NF after controlled potential electrolysis at 0.50 V vs. SHE.

Linear sweep voltammetry (LSV) and in situ Raman spectroscopy were used to study the formation of the Ni^{3+} species. The LSV sweep of NiB_x@NF in 1 M KOH shows an oxidation peak at 0.50 V vs. SHE, corresponds to the Ni^{2+}/Ni^{3+} oxidation (**Figure S2**). After electrolysis at 0.50 V vs. SHE, the surface of the NiB_x@NF was analysed by TEM (**Figures 1d‑i**) and XPS (**Figures. 1m‑o**). TEM images and TEM mapping demonstrated that a new shell was generated on the surface of the NiB_x particles (**Figures 1d, 1i**), while Ni $2p_{3/2}$, O 1s and B 1s XPS data indicated that this shell was composed of a mixture of Ni oxide and Ni hydroxide (**Figures 1m–o**). Raman spectra of the NiB_x@NF at 0.50 V vs. SHE showed the emergence of a Ni^{3+}-O bending peak at 471 cm^{-1} and a Ni^{3+}-O stretching peak at 554 cm^{-1}, demonstrating that NiOOH (Ni^{3+}) was the electrogenerated intermediate (**Figure 2a**).[7]

Initially, the oxidizability of Ni^{3+} for HMF oxygenation was computationally and experimentally investigated. The oxygenation of HMF to FDCA is a three-step process, includes the oxidation of the hydroxyl and aldehyde groups to carboxylic acids (**Figure S3**).[8] The oxidation of HMF to FDCA can proceed via two pathways, distinguished by the primary oxidation of the hydroxyl or carbonyl functionality (**Figure S3a**). The standard potential (E^o) for each step on both pathways were estimated using density functional theory (DFT) calculations (**Figure S3b**). HMF converts to 5-hydroxymethyl-2-furancarboxylic acid (HMFA) with an E^o of 0.098 V vs. SHE, while the competitive reaction from HMF to the dialdehyde 2,5-diformylfuran (DFF) has an E^o of −0.187 V vs. SHE. Further oxidation of the DFF and HMFA leads to the formation of 5-formyl-2-furancarboxylic acid (FFCA) with E^o of 0.119 V and −0.167 V vs. SHE, respectively. The final oxidation

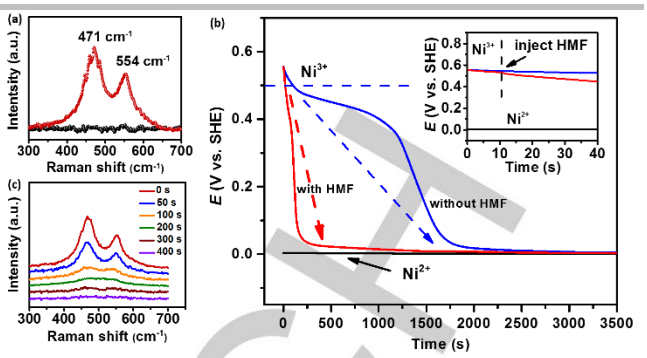

Figure 2. (a) Raman spectra of NiBx@NF at 0.50 V vs. SHE in 1 M KOH (red) and the as-prepared NiBx@NF (black); (b) Open-circuit potential versus time technique used to investigate the lifetime of the electrogenerated Ni^{3+} species on the surface of NiBx@NF in 1 M KOH with (red curve) and without (blue curve) HMF; (c) Changes in Raman spectra of NiBx@NF after the injection of HMF into the electrolyte.

of FFCA to FDCA occurs at an E^o of 0.109 V vs. SHE. The reduction potential of Ni^{3+}/Ni^{2+} is approximately 0.50 V vs. SHE.[9] Therefore, based on DFT calculations, the oxidizing ability of Ni^{3+} would be expected to drive each step during the oxidation of HMF to FDCA. Indeed, chemical oxygenation of HMF with the Ni^{3+}-complex $Ni_3O_2(OH)_4$[10] (**Figure S4**) showed a high yield (≥ 99 %) of FDAC in aqueous media. The powder X-ray diffraction (XRD) pattern of the Ni material after oxygenation demonstrated the formation of $Ni(OH)_2$, which is indicative of the Ni^{3+} to Ni^{2+} redox process responsible for the oxidation (**Figure S4**).

The activity of the electro-generated Ni^{3+} toward the oxygenation of HMF in 1 M KOH was further verified by an open-circuit potential versus time (OCPT) experiment. The change in the E_{OCP} reflects variations in the WE surface that, in turn, depend on changes in the active species at the electrode-solution interface. [11] In this work, E_{OCP} is associated with the anodic reaction occurring at the WE surface. The electro-generated Ni^{3+} species correspond to an E_{OCP} of 0.50 V vs. SHE, while the Ni^{2+} species correspond to an E_{OCP} of −0.01 V vs. SHE. The surface Ni was oxidized to Ni^{3+} at 0.50 V vs. SHE ($Ni(OH)_2 + OH^- \rightarrow NiOOH + H_2O + e^-$), followed by a spontaneous transition to Ni^{2+} ($NiOOH + H_2O + e^- \rightarrow Ni(OH)_2 + OH^-$) with a lifetime of 1700 s (**Figure 2b**). A control OCPT experiment showed that the lifetime of the electro-generated Ni^{3+} was shortened to 200 s upon adding HMF to the electrolyte (**Figures 2b, 2c**). This accelerated quenching indicates that the electrochemical generated Ni^{3+} is the active intermediate during the oxygenation of HMF.

The effect of water on the catalytic oxygenation of HMF with NiB_x@NF was assessed by performing trials in acetonitrile (**Figure S5**). The blank cyclic voltammogram (CV) curve obtained with NiB_x@NF in acetonitrile showed a Faradaic silent curve before 2.2 V vs. SHE, indicates difficulty in forming Ni^{3+} species without water. The subsequent addition of HMF gave an identical curve to that produced during the blank CV, indicating that HMF oxygenation did not proceed without the Ni^{3+} species. A control experiment with NiB_x@NF in acetonitrile with water produced a water oxidation current at 1.90 V vs. SHE, demonstrating the formation of Ni^{3+}. When water was added together with HMF, a current increase was observed at 1.70 V vs. SHE, assigned to the oxygenation of HMF. These results show that HMF was oxygenated, with water serving as the oxygen source, and that Ni^{3+} is an essential intermediate.

10.1002/anie.201903936

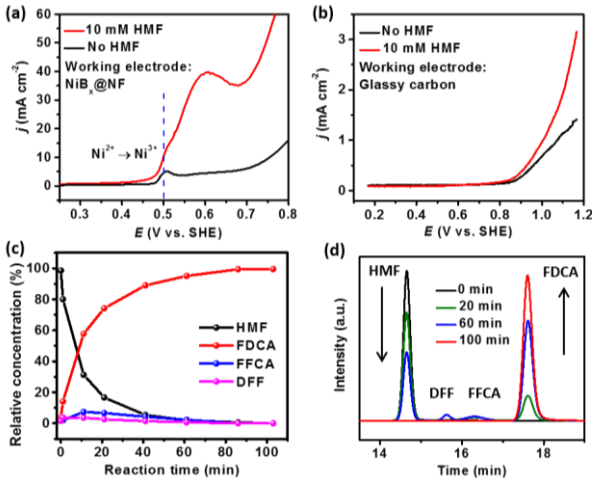

Figure 3. (a) LSV curves obtained from NiBx@NF in a 1 M KOH with and without HMF (10 mM); (b) LSV curves of a glassy carbon plate in a 1 M KOH with and without 10 mM HMF (scan rate, 5 mV s^{-1}); (c) the HMF, FDCA and intermediates concentrations vs. electrolysis time; (d) HPLC chromatograms acquired at various electrolysis times.

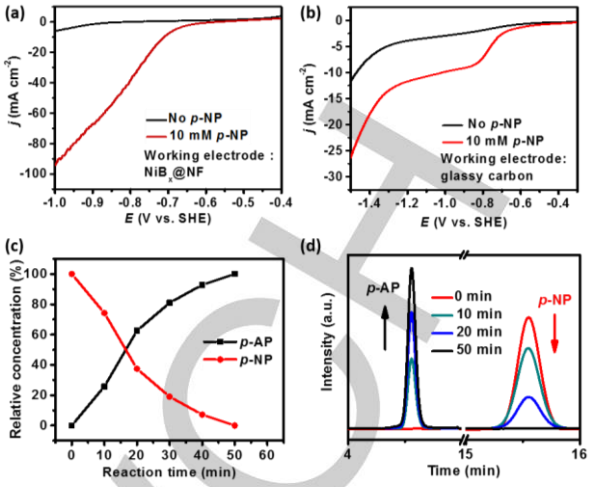

Figure 4. (a) LSV curves obtained from NiBx@NF in 1 M KOH in the absence and presence of 10 mM *p*-NP, at a scan rate of 5 mV s^{-1}; (b) polarization curves for a glassy carbon plate in 1 M KOH in the absence and presence of 10 mM *p*-NP, at a scan rate of 5 mV s^{-1}; (e) [*p*-NP] and [*p*-AP] vs. electrolysis time; (f) HPLC chromatograms acquired at various electrolysis time points.

Based on the previous results, we concluded that the electrocatalytic oxygenation of HMF with NiB_x@NF as WE and water as an oxygen source occurs through a two-step oxygen transfer mechanism (**Figure S6**). First, Ni^{2+} is electro-oxidized to Ni^{3+} with a newly bonded OH^- originating from water. Second, the resulting Ni^{3+} species, reacts with HMF, DFF and/or HMFA to produce FDCA, along with the regeneration of Ni^{2+}. In this process, water is the only oxygen source.

The electrocatalytic performance of NiB_x@NF toward HMF oxygenation in 1 M KOH is summarized in **Figure 3.** The LSV curve of NiB_x@NF without HMF shows a Ni^{2+}/Ni^{3+} oxidation peak at 0.50 V vs. SHE, followed by a silent region of 0.55–0.75 V vs. SHE, and the OER beyond 0.75 V vs. SHE.[12] To investigate the extent to which oxygenation was catalyzed, 10 mM HMF was added to the electrolyte. The LSV curve shows a similar Ni^{2+}/Ni^{3+} process at 0.50 V vs. SHE, followed by a significant enhancement at 0.60 V vs. SHE with a peak current density of 40 mA cm^{-2}, which is attributed to the HMF oxygenation reaction (**Figure 3a**). It is evident that HMF oxygenation is favoured over the OER. Furthermore, the current density beyond 0.70 V vs. SHE is attributed to the superposition of HMF oxygenation and the OER. Control experiments with a glassy carbon plate produced a Faradaic silent region from 0.20 to 0.80 V vs. SHE both with and without the HMF (**Figure 3b**). These results indicate that the NiB_x@NF promoted HMF oxygenation through a electrocatalytic process. Further research showed that the peak current densities at 0.60 V vs. SHE increased linearly along with increases in the HMF concentration (**Figures S7**). These results suggest that the oxygenation on the WE surface is a diffusion-controlled process.

Conversion, selectivity and Faradaic efficiency are investigated during the oxygenation of HMF to FDCA by chronoamperometry. A constant potential of 0.60 V vs. SHE was applied during the electrolysis (**Figure 3c, 3d**). The reaction process was monitored by high performance liquid chromatography (HPLC). The results showed that HMF was 99.8 ± 0.2% converted to FDCA after 100 min. DFF and FFCA were identified by HPLC as intermediates. Overall, the oxygenation of HMF to FDCA is a six electron process,[8,3d] and the Faradaic efficiency of the electrocatalytic HMF oxygenation was approximately 99.5 ± 0.5%, based on the electrolysis and the theoretical charges for the formation of FDCA (**Figure S8**).

To enhance atom utilization, a cathodic reaction is necessary to consume the protons generated during the oxygenation of HMFThe hydrogenation of nitro-compounds to their corresponding amines is important for the synthesis of fine chemicals, such as dyes and pigments.[13] In subsequent trials, the hydrogenation of *p*-NP to *p*-AP was used as a model reaction in conjunction with NiB_x/NF as the WE and water as the hydrogen source.

The electro-catalytic hydrogenation of *p*-NP proceeds via three two-electron-two-proton processes (**Figure S9**). Under standard conditions, ΔG was found to be negative (ΔG < 0) for each step, indicating that the hydrogenation of *p*-NP is an exergonic process. The reduction potentials for the continuous reduction reactions are 0.603, 0.333 and 0.719 V vs. SHE ($R^2NO_2 + 2H^+ + 2e^- \rightarrow R^2NO + H_2O$, $R^2NO + 2H^+ + 2e^- \rightarrow R^2NHOH$, $R^2NHOH \rightarrow R^2NH + H_2O$, $R^2NH + 2H^+ + 2e^- \rightarrow R^2NH_2$, R^2NO_2 = *p*-nitrophenol), and thus occur prior to hydrogen evolution on a thermodynamic basis. These calculations demonstrate that the reduction of nitrosamine to hydroxylamine requires the highest potential of 0.333 V vs. SHE.

In 1 M KOH, NiB_x/NF showed an onset potential of –0.90 V vs. SHE for HER (**Figure 4a**). After the addition of *p*-NP, the LSV curve exhibited an onset potential of –0.60 V vs. SHE, followed by a current density of –40 mA cm^{-2} at –0.83 V vs. SHE (0 V vs. RHE). The increased current density beyond –0.90 V vs. SHE is attributed to the superposition of the hydrogenation reaction and the HER. These results indicate that the targeted nitro-group hydrogenation occurred prior to the HER, and that a high Faradaic efficiency can readily be achieved through controlling the applied potential. Control experiments with a glassy carbon electrode showed a similar activity toward *p*-NP hydrogenation with an onset potential of –0.65 V vs. SHE (**Figure 4b**). It is evident that the hydrogenation of *p*-NP in 1 M KOH proceeds on an electro-reduction mechanism. [14] Furthermore, a linear relationship was observed between the *p*-NP concentration and the corresponding

10.1002/anie.201903936

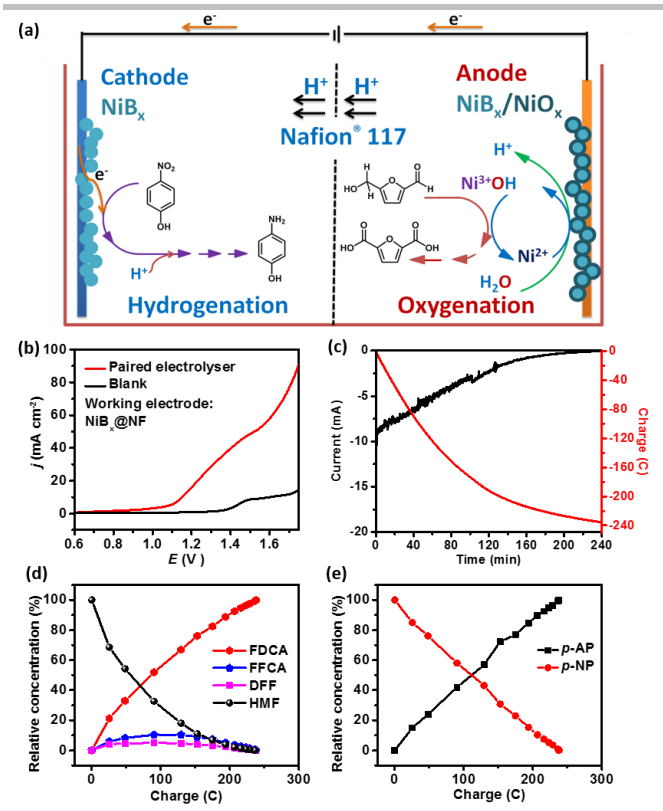

Figure 5. (a) Schematic representation of the paired electrochemical cell; (b) the LSV curves obtained from the paired electrolyser in 1.0 M KOH in the absence and presence of organic reactants (scan rate, 5 mV s^{-1}); (c) current–time and charge–time transients during constant potential electrolysis at 1.40 V; (d) results from analysis of the anode side at various charges; (e) results from analysis of the cathode side at various charges.

current density (**Figure S10**), indicating a molecular diffusion reaction process. The catalytic properties of NiB_x@NF during the hydrogenation of *p*-NP were further explored by chronoamperometry. A conversion and selectivity of ≥99% was achieved after 50 min at the applied potential of −0.83 V vs. SHE (**Figures 4c, 4d, S11**). During the catalytic process, no intermediates were observed by HPLC. A Faradaic efficiency of approximately 99% was calculated by comparing the charge consumed in the production of *p*-AP with the integrated current.

Paired electrolysis combines two desirable half-reactions to maximize energy efficiency and the formation of useful products.[15] As previously described, the as-prepared NiB_x@NF exhibited promising catalytic performance during the electrocatalytic oxygenation and hydrogenation half reactions under the same conditions. Hence, we integrated these two half-reactions in an electrolyser to realize paired electrolysis, using the full potential of water as both an oxygen and hydrogen source (**Figure 5a**). The catalytic activities of NiB_x@NF during HMF oxygenation and *p*-NP hydrogenation in the paired electrolyser were further evaluated by acquiring polarization curves and electrolysis (**Figure 5**). In the absence of HMF and *p*-NP, NiB_x@NF exhibited HER activity beyond 1.65 V (**Figure 5b**). The LSV curve obtained during the paired oxygenation of HMF and hydrogenation of *p*-NP (**Figure 5b**) exhibited an onset potential of 1.10 V and reached a plateau of 50 mA cm^{-2} at 1.5 V. These results indicate that the paired reactions proceeded preferentially rather than the hydrogen evolution.

An applied potential of 1.40 V was used for further chronoamperometric tests. In the electrolysis process, the Faradaic current density gradually decreased to 0 within 240 min, with a charge build-up of 238 C (**Figure 5c**). The starting substrates (HMF and *p*-NP) were consumed with ≥99% conversion to the corresponding products (**Figures 5d, 5e**). The expected intermediates FFCA and DFF, were also detected by HPLC (**Figure 5d**). Furthermore, a Faradaic efficiency of ≥99% was achieved for each side.

The design of the paired electrolyser is scalable to meet different requirements. A simple photoelectrochemical-driven oxygenation and hydrogenation device was created by connecting solar cells (1.5 V silicon solar panel) and the paired electrolyser in series (**Figure S12**). This photovoltaic integrated electrolyser demonstrated the simultaneous oxygenation of HMF and hydrogenation of *p*-NP in an aqueous solution under outdoor sunlight with high conversion and selectivity (≥99%). In addition, high conversion and selectivity were also observed when HMF was replaced with furan-2-carbaldehyde, furan-2-ylmethanol, pyridine-4-ylmethanol and 4-(hydroxymethyl)phenol as the compounds undergoing oxygenation, and when *p*-NP was replaced with *m*-NP, *o*-NP, 4-nitrobenzonitrile and 1-ethynyl-4-nitrobenzene (**Figure S13, S14** and **Table S1**).

In summary, we have developed a paired electrochemical system for the oxygenation and hydrogenation of organics to replace the chemical-driven stoichiometric reactions using sacrificial reagents. Water was found to be essential as the oxygen and hydrogen source for these redox reactions in the paired electrolyser. The as-designed electrochemical cell exhibit high conversion, selectivity and Faradaic efficiency values at both the anode and cathode simultaneously, without the involvement of oxygen and hydrogen. As an example, a conversion efficiency of ≥99% was achieved during the oxygenation of HMF to FDCA and the hydrogenation of *p*-NP to *p*-AP. The experimental results show that this paired electrolyser can be extended to other organic substrates. This new (photo)electrocatalytic cell system is very promising and should have practical applications in future green chemical systems using electricity or sunlight as the energy input and water as both the oxygen and hydrogen sources.

Experimental Section

All electrochemical experiments were performed with a CH Instrument 660E potentiostat. The electrochemical cell contained the sample as a WE, a platinum foil (4 cm^2) as an auxiliary electrode and Hg/HgO (1 M KOH, Tjaida) as a reference electrode ($E^o_{Hg/HgO}$ = 0.098 V vs. SHE). The reference electrodes were calibrated by measuring the standard hydrogen electrode (SHE) potential. Potentials were converted to SHE via the Nernst equation: $E_{SHE} = E_{Hg/HgO} + 0.059\ pH + E^o_{Hg/HgO}$. The internal resistance between the reference and WE (R_u) was determined by the automatic current interrupt (R_u = 0.8 ± 0.1 Ω). *i*R compensation during LSV sweeps was performed using the automatic current interrupt method, with a value of 75%×R_u. Chronopotentiometry measurements were performed under Argon atmosphere (unless stated otherwise) with an H-type cell to evaluate the catalytic activity. Nafion® 117 membranes were used to separate the anodic and cathodic compartments.

Acknowledgements

10.1002/anie.201903936

We acknowledge the financial support of this work by Swedish Energy Agency, the Knut & Alice Wallenberg Foundation (KAW 2016.0072), the Swedish Research Council (2017-00935), the National Basic Research Program of China (973 Program, 2014CB239402) and the Fundamental Research Funds for the Central Universities (DUT17RC(3)083).

Keywords: electrosynthesis • water • oxygenation • hydrogenation • green chemical synthesis

[1] D. A. Bryant, N. U. Frigaard, *Trends Microbiol.* **2006**, *14*,488–496.

[2] S. G. Sligar, T. M. Makris, I. G. Denisov, *Biochem. Biophys. Res. Commun.* **2005**, *338*, 346–54.

[3] a) B. You, N. Jiang, X. Liu, Y. Sun, *Angew. Chem. Int. Ed.* **2016**, *55*, 9913–9917; b) N. Jiang, B. You, R. Boonstra, I. M. T. Rodriguez, Y. Sun, *ACS Energy Lett.* **2016**, *1*, 386–390; c) B. You, N. Jiang, M. Sheng, M. W. Bhushan, Y. Sun, *ACS Catal.* **2016**, *6*, 714–721; d) S. Barwe, J. Weidner, S. Cychy, D. M. Morales, S. Dieckhöfer, D. Hiltrop, J. Masa, M. Muhler, W. Schuhmann, *Angew. Chem. Int. Ed*. **2018**, *57*, 11460–11464; e) W. Liu, L. Dang, Z. Xu, H. Yu, S. Jin, G. W. Huber, *ACS Catal.* **2018**, *8*, 5533–5541; f) D. J. Chadderdon, L. Xin, J. Qi, Y. Qiu, P. Krishna, K. L. More, W. Li, *Green Chem.* **2014**, *16*, 3778–3786.

[4] a) M. G. Walter, E. L. Warren, J. R. McKone, S. W. Boettcher, Q. Mi, E. A. Santori, N. S. Lewis, *Chem. Rev.* **2010**, *110*, 6446–6473; b) Li, K., & Sun, Y. *Chem. Eur. J.* **2018**, *24*, 18258–18270.

[5] P. Zhang, M. Wang, Y. Yang, T. Yao, H. Han, L. Sun, *Nano Energy* **2016**,*19*, 98–107.

[6] a) A. P. Grosvenor, M. C Biesinger, R.St.C. Smart, N. S. McIntyre, *Surf. Sci.* **2006**, *600*, 1771–1779; b) J. Legrand, A. Taleb, S. Gota, M.-J. Guittet, C. Petit, *Langmuir* **2002**,*18*, 4131–4137.

[7] B. S. Yeo, A. T. Bell, *J. Phys. Chem. C* **2012***, 116*, 8394–8400.

[8] Z. Zhang, G. W. Huber, *Chem. Soc. Rev.* **2018**, 47, 1351–1390.

[9] a) L. Hu, Z. Yu, Z. Hu,Y. Song, F. Zhang, H. Zhu,S. Jiao, *Electrochim. Acta* **2015**, *174*, 273–281; b) M. J. Grill, J. Ogle, A. Stephen, S. A. Miller, S. A. *J. Org. Chem.* **2006**, *71*, 9291–9296.

[10] B. Polteau, F. Tessier, F. Cheviré, L. Cario, F. Odobel, S. Jobic *Solid State Sci.* **2016**, *54*,37–42.

[11] Liu, T., Conway, B. E. *J. Appl. Electrochem.* **1987**, *17*, 983–996.

[12] J. Jiang, M. Wang, W. Yan, X. Liu, J. Liu, J. Yang, L. Sun, *Nano Energy* **2017**, *38*, 175–184.

[13] a) A. Goyal, S. Bansal, S. Singhal, *Int. J Hydrog. Energy* **2014***, 39*, 4895–908; b) B. Dutta, S. Biswas, V. Sharma, N. O. Savage, S. P. Alpay, S. L. Suib, *Angew. Chem. Int. Ed.* **2016**, *55*, 2171–2175; c) D. Iranshahi, E. Pourazadi, A. M. Bahmanpour, M.R. Rahimpour, *Int J. Hydrog. Energy* **2011**, *36*, 3483–3495.

[14] a) C. L. Forryan, R. G. Compton, *Phys. Chem. Chem. Phys.* **2003**, *5*, 4226–4230; b) S. Möhle, M. Zirbes, E. Rodrigo, T. Gieshoff, A. Wiebe, S. R. Waldvogel, *Angew. Chem. Int. Ed*. **2018**, *57*, 2–26.

[15] a) M. Yan, Y. Kawamata, P. S. Baran, *Chem. Rev.* **2017**, *117*, 13230–13319; b) R. S. herbo, R. S. Delima, V. A. Chiykowski, B. P. MacLeod, C. P. Berlinguette, R. S. Sherbo, *Nature Catal.* **2018**, *1*, 501–507.

10.1002/anie.201903936

WILEY-VCH

Layout 1:

COMMUNICATION

NiB_x@NF was employed as both an anode and cathode in a paired electrosynthesis cell for the respective oxygenation and hydrogenation of organics, with water as both the oxygen and hydrogen source. Conversions efficiencies and selectivities of ≥99% were achieved during the oxygenation of 5-hydroxymethylfurfural and the simultaneous hydrogenation of *p*-nitrophenol.

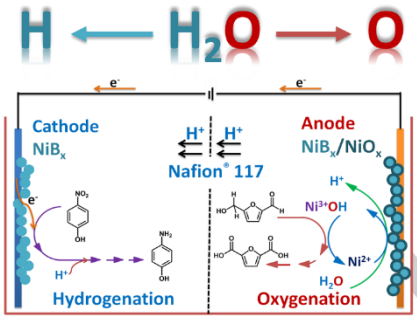

*Peili Zhang, Xia Sheng, Xiaoyu Chen, Zhiyong Fang, Jian Jiang, Mei Wang, Fusheng Li, Lizhou Fan, Yansong Ren, Biaobiao Zhang, Brian J.J. Timmer, Mårten S.G.Ahlquist, Licheng Sun**

Page No. – Page No.

Paired electrocatalytic oxygenation and hydrogenation of organic substrates using water as oxygen and hydrogen source